9374–9388 *Nucleic Acids Research, 2021, Vol. 49, No. 16* *Published online 14 August 2021*
https://doi.org/10.1093/nar/gkab646

Photo-activatable Ub-PCNA probes reveal new structural features of the *Saccharomyces cerevisiae* Polη/PCNA complex

Siqi Shen, Gregory A. Davidson, Kun Yang and Zhihao Zhuang*

Department of Chemistry and Biochemistry, University of Delaware, 214A Drake Hall, Newark, DE 19716, USA

Received November 05, 2020; Revised July 02, 2021; Editorial Decision July 09, 2021; Accepted August 12, 2021

ABSTRACT

The Y-family DNA polymerase η (Polη) is critical for the synthesis past damaged DNA nucleotides in yeast through translesion DNA synthesis (TLS). TLS is initiated by monoubiquitination of proliferating cell nuclear antigen (PCNA) and the subsequent recruitment of TLS polymerases. Although individual structures of the Polη catalytic core and PCNA have been solved, a high-resolution structure of the complex of Polη/PCNA or Polη/monoubiquitinated PCNA (Ub-PCNA) still remains elusive, partly due to the disordered Polη C-terminal region and the flexibility of ubiquitin on PCNA. To circumvent these obstacles and obtain structural insights into this important TLS polymerase complex, we developed photo-activatable PCNA and Ub-PCNA probes containing a p-benzoyl-L-phenylalanine (*p*Bpa) crosslinker at selected positions on PCNA. By photo-crosslinking the probes with full-length Polη, specific crosslinking sites were identified following tryptic digestion and tandem mass spectrometry analysis. We discovered direct interactions of the Polη catalytic core and its C-terminal region with both sides of the PCNA ring. Model building using the crosslinking site information as a restraint revealed multiple conformations of Polη in the polymerase complex. Availability of the photo-activatable PCNA and Ub-PCNA probes will also facilitate investigations into other PCNA-containing complexes important for DNA replication, repair and damage tolerance.

GRAPHICAL ABSTRACT

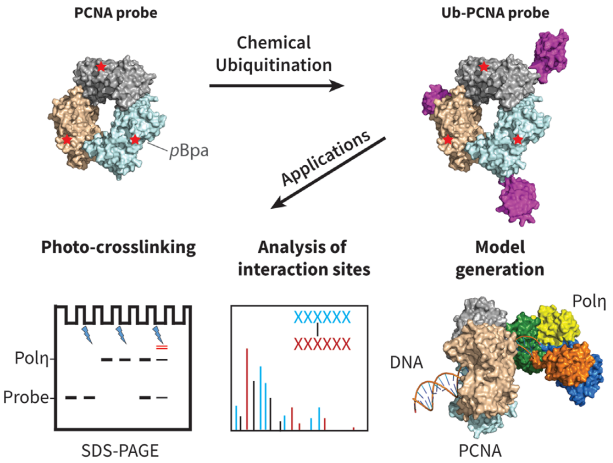

INTRODUCTION

Polymerase η (Polη) belongs to the Y-family DNA polymerases and is evolutionarily conserved in eukaryotes (1–6). Mutation of human Polη is associated with xeroderma pigmentosum variant (XPV) (7,8). XPV patients face an increased chance of skin cancer when being exposed to sunlight (7,8). Polη contains a ubiquitin-binding zinc-finger domain (UBZ) and is recruited to the DNA damage site following the monoubiquitination of PCNA (9–11). It plays an important role in bypassing cyclobutane pyrimidine dimer (CPD) and 8-oxoguanine in translesion DNA synthesis (TLS) (12–16). Although crystal structures of the human and yeast Polη catalytic core (17–24) and a low-resolution electron microscopy (EM) structure of the human Polη/Ub-PCNA complex (25) were reported, a high-resolution structure of the full-length Polη in complex with PCNA or Ub-PCNA still remains elusive.

PCNA interacts with a large group of proteins and serves as a hub for cellular DNA replication, repair and damage tolerance (26). PCNA is a structurally conserved and ring-shaped homotrimeric protein that encircles DNA (27). It is a central component of the replication fork in eukaryotes

*To whom correspondence should be addressed. Tel: +1 302 831 8940; Email: zzhuang@udel.edu

and archaea (26). The PCNA ring has two sides with the front side facing the direction of DNA replication and containing an inter-domain connecting loop (IDCL) (28–30). The IDCL is adjacent to a hydrophobic pocket on PCNA that is important for PCNA's interaction with its partner proteins. It is known that many PCNA-interacting proteins engage PCNA at its front side. Nonetheless, structural elements at the back side of the PCNA ring, such as loop J in the yeast PCNA (a.a. 105–110), were reported to be required for Polη's normal function in TLS (31–33).

Ubiquitin (Ub) is highly conserved in eukaryotes. Ubiquitination represents a major type of protein post-translational modification (34). Ub can be covalently attached to the acceptor protein through a cascade (E1-E2-E3) of enzymatic reactions (35). Ubiquitination is known to play important roles in protein degradation, transcription regulation, immune response and DNA damage tolerance (36–38). Many TLS polymerases contain ubiquitin-binding domains (UBD) that are required for their interactions with Ub (5,6,39). In yeast *Saccharomyces cerevisiae,* following DNA damage, monoubiquitination of PCNA at Lys164 by Rad6/Rad18 activates TLS by recruiting specialized DNA polymerases which in turn bypass the DNA lesion (11,40–44). PCNA can be further polyubiquitinated through K63-linked ubiquitin chain by Ubc13-Mms2/Rad5 in yeast, which is thought to be involved in error-free lesion bypass (30,45–47).

Polη in yeast and human contains an N-terminal polymerase catalytic core and a C-terminal regulatory region with an embedded UBD (3,5,6). Polη's catalytic core consists of fingers, palm, thumb and little finger (LF, also known as polymerase-associated domain or PAD) domains (Figure 1A). The C-terminal region of yeast Polη contains a ubiquitin-binding zinc finger (UBZ, a.a. 549–582) and a conserved PCNA-interacting protein box (PIP, a.a. 621–628). A Langevin dynamics simulation suggested that a large part of the yeast Polη C-terminal region (a.a. 523–549 and 580–632) is unstructured (48). The PIP box is well characterized for Polη's interaction with PCNA (5,26,49). A recent NMR study suggested that the PIP box in yeast Polη also contributes to its interaction with Ub (50).

Despite extensive studies, the molecular mechanism of TLS is still not fully understood. A TLS model in which the replicative and TLS DNA polymerases engage the same sliding clamp (PCNA or β-clamp) simultaneously and trade their position on DNA is supported by studies in reconstituted systems (51–53). Further X-ray crystal structure determination of a split yeast Ub-PCNA has led to a model of the Polη/Ub-PCNA complex in which the C-terminal region of Polη is juxtaposed to the conjugated Ub at the back side of PCNA while the polymerase catalytic core is positioned at the PCNA front side bound to DNA (54). This model was further supported by solution structure study of the full-length Polη by small angle X-ray scattering (SAXS) that revealed a high degree of flexibility of the unstructured Polη C-terminal region (48). This conformational flexibility was thought to facilitate the polymerase switching between the replicative and TLS polymerases tethered to the PCNA ring simultaneously. Notably, a 22 Å resolution structure of human Polη/Ub-PCNA/DNA structure was obtained by combining glutaraldehyde chemical crosslinking and single-particle electron microscopy (25). This structure revealed that one of the ubiquitins on PCNA adopts a 'flipped-out' conformation while interacting with the C-terminal region of Polη in the complex. In a human Ub-PCNA crystal structure, Ub was found to adopt an extended conformation on the PCNA ring (55). In prokaryotes, several Y-family DNA polymerases have also been investigated extensively (1,2,5).

To address the conformational flexibility of Polη in complex with PCNA or Ub-PCNA, we combined photo-crosslinking and mass spectrometry to obtain structural insights into this potentially dynamic TLS complex. A photoreactive unnatural amino acid *p*-benzoyl-L-phenylalanine (*p*Bpa) (56) is incorporated into yeast PCNA at selected positions. Chemical ubiquitination was used to generate the corresponding Ub-(*p*Bpa)PCNA probes (57,58). We chose a number of residues on PCNA for the incorporation of *p*Bpa in order to interrogate the potential interactions between the full-length Polη and both sides of the PCNA ring. Our crosslinking results showed that the introduction of *p*Bpa on the front side of PCNA, such as positions 125 and 254, resulted in an efficient crosslinking with Polη. Interestingly, we also obtained direct evidence of Polη's interaction with the back side of PCNA through *p*Bpa introduced at positions 108 and 245. By mass spectrometry analysis of photo-crosslinked peptides, multiple new interaction sites on the catalytic core of Polη were revealed. We also uncovered interactions between the Polη C-terminal disordered region and different sites on PCNA, suggesting flexibility of the C-terminal Polη region in the complex.

MATERIALS AND METHODS

Protein expression and purification

A cysteine-light K164C PCNA (C22S/C30S/C62S/C81S/K164C PCNA) (59) was cloned into pET-15b vector for generation of the PCNA probes. QuikChange PCR was used to introduce TAG amber codon (for genetic incorporation of *p*Bpa) as well as mutation (F245A, L126A/I128A or P252A/K253A) into the cysteine-light K164C PCNA. QuikChange PCR was also used to introduce TAG amber codon for genetic incorporation of *p*Bpa into Ub and to introduce M518A/F519A mutation into the full-length Polη (Polη^{FL}) or a TAG stop codon into Polη^{FL} for generating the truncated Polη$_{1–513}$ (Polη^{CC}) and Polη$_{1–523}$.

For the *p*Bpa-containing PCNA expression and purification, the PCNA protein expression plasmid was co-transformed with a tRNA synthetase/tRNA pair-containing plasmid pEVOL-pBpF (Addgene #31190, a gift from Peter Shultz) (56) into *Escherichia coli* BL21(DE3) cells for the expression of (*p*Bpa)PCNA. Co-transformed cells were grown in terrific broth (TB) media with 100 μg/ml ampicillin and 34 μg/ml chloramphenicol. In a typical (*p*Bpa)PCNA protein expression and purification, *E. coli* BL21(DE3) cells were spun down when OD_{600} reached 0.8 and resuspended in a 5-fold less volume TB media in the presence of 1 mM *p*Bpa (AEchem), 100 μg/ml ampicillin and 34 μg/ml chloramphenicol. Resuspended cells

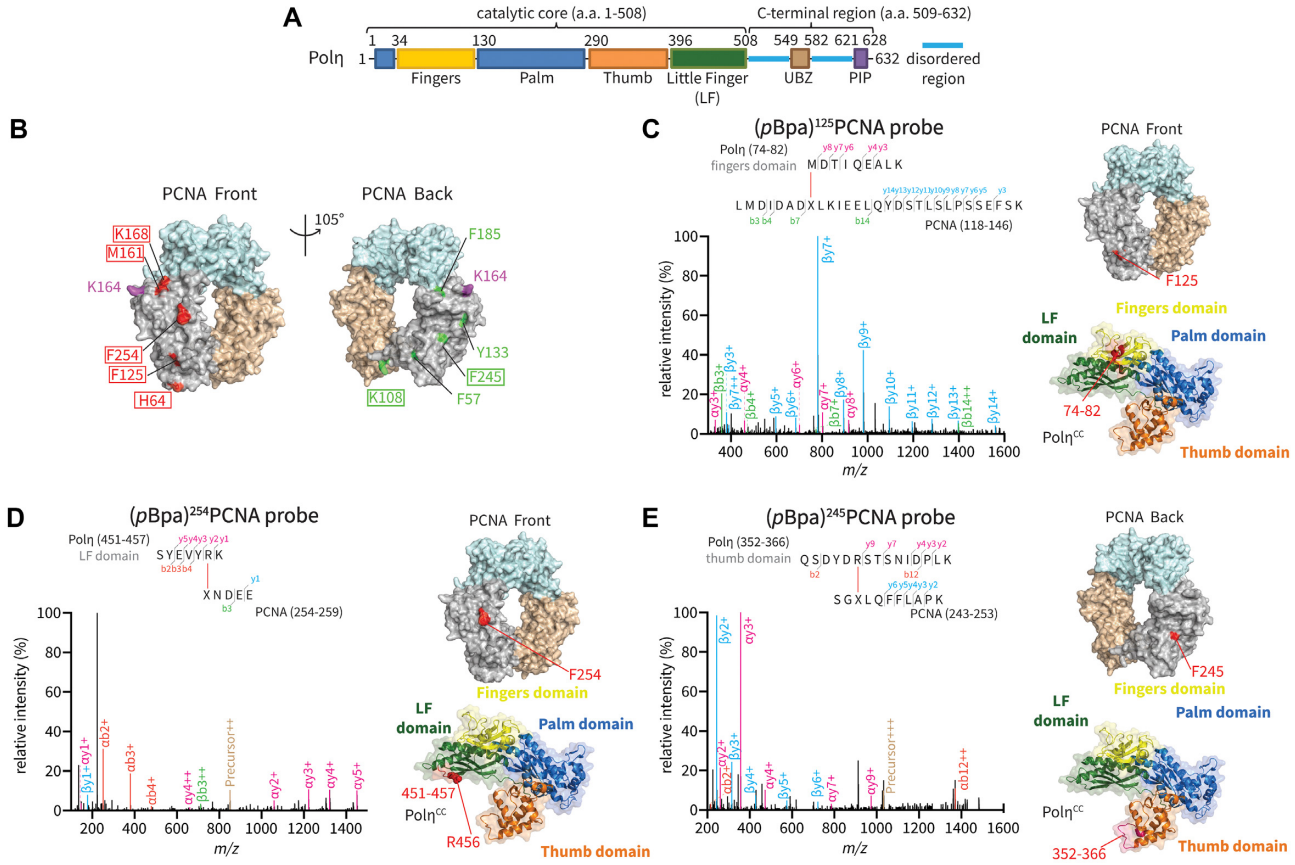

Figure 1. Photo-crosslinking of (*p*Bpa)PCNA probes with the full-length Polη. (**A**) Illustration of the domain structure of the full-length Polη. (**B**) The front- and back-side view of PCNA trimer with *p*Bpa incorporation site highlighted in red or green. The sites that showed successful photo-crosslinking with Polη were highlighted with a box. (**C**) A representative MS/MS spectrum of a peptide (a.a. 74–82) in the Polη fingers domain crosslinked to a PCNA peptide containing ^{125}*p*Bpa. X represents *p*Bpa. (**D**) A representative MS/MS spectrum of a peptide (a.a. 451–457) on the Polη LF domain crosslinked to a PCNA peptide containing ^{254}*p*Bpa. X represents *p*Bpa. (**E**) A representative MS/MS spectrum of a peptide (a.a. 352–366) in the Polη thumb domain crosslinked to a PCNA peptide containing ^{245}*p*Bpa. X represents *p*Bpa. Yeast PCNA (PDB: 1PLQ) and Polη^{CC} (PDB: 2R8K) structures are shown.

were grown at 16°C for 1 h followed by the addition of 0.5 mM IPTG and 0.02% (w/v) arabinose for inducing protein expression at 16°C for 24 h. Harvested cell pellet was resuspended and lysed by sonication at 4°C in a lysis buffer containing 50 mM sodium phosphate (pH 8.0), 5% glycerol, 500 mM NaCl, 10 mM imidazole and 1 mM PMSF. The crude extract was spun down by centrifugation and the supernatant was bound to HisPur cobalt resin (Thermo Fisher Scientific) for 2 h at 4°C. The bound resin was washed with the lysis buffer and then eluted with a 50 mM sodium phosphate buffer (pH 8.0) containing 5% glycerol, 100 mM NaCl and 200 mM imidazole. The eluted protein was directly loaded to a HiTrap Q anion exchange column (GE Healthcare Life Sciences) in a 50 mM sodium phosphate buffer (pH 8.0) containing 5% glycerol, 100 mM NaCl and 1 mM DTT. Proteins were eluted with a 100–600 mM NaCl gradient in a 50 mM sodium phosphate buffer (pH 8.0) containing 5% glycerol and 1 mM DTT. The peak fractions were collected, concentrated and buffer exchanged into a buffer containing 50 mM Tris-HCl (pH 7.5), 10% glycerol, 50 mM NaCl and 1 mM DTT.

For mutant PCNA expression, *E. coli* Rosetta(DE3) cells transformed with mutant PCNA/pET-15b plasmid were cultured in TB medium at 37°C in the presence of 100 μg/ml ampicillin and 34 μg/ml chloramphenicol. The cell culture was induced with 0.5 mM IPTG at OD_{600} 0.6 and further cultured for 16 h at 16°C. Harvested cell pellet was resuspended and lysed by sonication at 4°C in a lysis buffer containing 50 mM sodium phosphate (pH 8.0), 5% glycerol, 500 mM NaCl, 10 mM imidazole and 1 mM PMSF. The crude extract was spun down by centrifugation and the supernatant was bound to HisPur cobalt resin (Thermo Fisher Scientific) for 2 h at 4°C. The bound resin was washed with the lysis buffer and then eluted with a 50 mM sodium phosphate buffer (pH 8.0) containing 5% glycerol, 100 mM NaCl and 200 mM imidazole. Eluted fractions containing PCNA were collected, concentrated and buffer exchanged into a buffer containing 50 mM Tris-HCl (pH 7.5), 10% glycerol, 50 mM NaCl and 1 mM DTT.

For expression and purification of Polη^{FL} and Polη^{FL} (M518A/F519A), Rosetta(DE3) cells transformed with the individual Polη gene, i.e. Polη^{FL}, Polη^{FL} (M518A/F519A), in pET-28a vector were cultured in TB medium at 37°C in the presence of 50 μg/ml kanamycin and 34 μg/ml chloramphenicol. The cell culture was induced with 0.5 mM IPTG when OD_{600} reached 0.6 and further cultured at 16°C for 16 h. In a typical purification, cells were harvested and lysed by sonication in a lysis buffer containing 50 mM

sodium phosphate (pH 7.4), 7% glycerol, 300 mM NaCl, 10 mM imidazole and 1 mM PMSF. The supernatant was bound to HisPur cobalt resin (Thermo Fisher Scientific) for 2 h at 4°C. The resin was washed with the lysis buffer and eluted with a buffer containing 50 mM sodium phosphate (pH 7.4), 7% glycerol, 100 mM NaCl, and 200 mM imidazole. The eluted protein was buffer exchanged to a buffer containing 50 mM Tris-HCl (pH 7.4), 5% glycerol, 50 mM NaCl, 1 mM DTT and loaded onto a HiTrap SP cation exchange column (GE Healthcare Life Sciences). The protein was eluted with a 50–600 mM NaCl gradient in a buffer containing 50 mM Tris-HCl (pH 7.4), 5% glycerol and 1 mM DTT. The peak fractions containing Polη were collected and directly loaded onto a HiTrap Heparin HP column (GE Healthcare Life Sciences). Proteins were eluted with a 50–800 mM NaCl gradient in a buffer containing 50 mM Tris-HCl (pH 7.4), 5% glycerol and 1 mM DTT. The peak fractions containing Polη were collected, concentrated and buffer exchanged into a buffer containing 50 mM Tris-HCl (pH 7.5), 5% glycerol, 50 mM NaCl and 1 mM DTT.

For Polη^{CC} and Polη$_{1–523}$ expression, Rosetta(DE3) cells transformed with the individual Polη gene, i.e. Polη^{CC} and Polη$_{1–523}$, in pET-28a vector were cultured in TB medium at 37°C in the presence of 50 μg/ml kanamycin and 34 μg/ml chloramphenicol. The cell culture was induced with 0.5 mM IPTG when OD_{600} reached 0.6 and further cultured at 16°C for 16 h. In a typical purification, cells were harvested and lysed by sonication in a lysis buffer containing 50 mM sodium phosphate (pH 6.5), 7% glycerol, 300 mM NaCl, 10 mM imidazole and 1 mM PMSF. The supernatant was bound to HisPur cobalt resin (Thermo Fisher Scientific) for 2 h at 4°C. The resin was washed with the lysis buffer and eluted with a buffer containing 50 mM sodium phosphate (pH 6.5), 7% glycerol, 100 mM NaCl and 200 mM imidazole. The eluted protein was buffer exchanged to a 50 mM sodium phosphate buffer (pH 6.5) containing 5% glycerol, 50 mM NaCl, 1 mM DTT and loaded onto a HiTrap Heparin HP column (GE Healthcare Life Sciences). Proteins were eluted with a 50–800 mM NaCl gradient in a 50 mM sodium phosphate buffer (pH 6.5) containing 5% glycerol and 1 mM DTT. The peak fractions containing Polη were collected, concentrated and buffer exchanged into a buffer containing 50 mM Tris-HCl (pH 7.5), 5% glycerol, 50 mM NaCl and 1 mM DTT.

The expression and purification of Ub_{1-75}-intein fusion for generation of Ub-PCNA probes was based on a previously published method (58). Ub_{1-75}-intein was expressed in BL21(DE3) cells in TB medium at 37°C in the presence of 100 μg/ml ampicillin. Cells were induced by 1 mM IPTG when OD_{600} reached 0.8 at 16°C for 16 h. Cells were harvested and lysed by sonication in a buffer containing 20 mM Tris-HCl (pH 7.5), 5% glycerol, 200 mM NaCl and 1 mM EDTA. The supernatant was bound to chitin resin (New England Biolabs) for 16 h at 4°C. The bound resin was washed with a buffer containing 20 mM Tris-HCl (pH 7.5), 5% glycerol, 1 M NaCl and 1 mM EDTA and equilibrated with a buffer containing 50 mM MES (pH 6.5) and 100 mM NaCl. After equilibration, the bound protein was cleaved in a buffer containing 50 mM MES (pH 6.5) and 100 mM NaCl supplemented with 75 mM β-mercaptoethanesulfonic acid sodium salt (MESNA, TCI chemicals) for 16 h at room temperature. Eluted protein was buffer exchanged to a buffer containing 50 mM MES (pH 6.5) and 100 mM NaCl to remove excessive amount of MESNA.

For the *p*Bpa-containing Ub expression, the amber codon-containing Ub_{1-75}-intein pTYB1 expression plasmid was co-transformed with pEVOL-pBpF into *E. coli* BL21(DE3) cells. Co-transformed cells were grown in terrific broth (TB) media with 100 μg/ml ampicillin and 34 μg/ml chloramphenicol. Cells were spun down when OD_{600} reached 0.8 and resuspended in a 5-fold less volume TB media in the presence of 1 mM *p*Bpa (AEchem), 100 μg/ml ampicillin and 34 μg/ml chloramphenicol. Resuspended cells were grown at 16°C for 1 h followed by the addition of 0.5 mM IPTG and 0.02% (w/v) arabinose for protein expression at 16°C for 24 h. Purification of (*p*Bpa)Ub was carried out following the same procedure as Ub_{1-75} described above.

Generation of Ub-(*p*Bpa)PCNA probes for photo-crosslinking

Purified (*p*Bpa)PCNA and Ub were covalently conjugated by a chemical ubiquitination method to generate the non-cleavable Ub-(*p*Bpa)PCNA probe. A non-cleavable linker (NCL) was used for the chemical ubiquitination of (*p*Bpa)PCNA following a previously published method (58). Ub_{1-75} was expressed and purified as an Ub_{1-75}-intein fusion, followed by cleavage using a buffer containing 50 mM MES (pH 6.5), 100 mM NaCl and 75 mM MESNA to yield Ub_{1-75}-MESNA. Cleaved protein was buffer exchanged to a buffer containing 50 mM MES (pH 6.5) and 100 mM NaCl to remove excess amount of MESNA. A non-cleavable linker (NCL) synthesized as previously described (57) was reacted with Ub_{1-75}-MESNA in a buffer containing 50 mM MES (pH 6.5), 100 mM NaCl in a typical molar ratio of 800:1 to generate Ub_{1-75}-NCL. Ub_{1-75}-NCL was deprotected by adding an equal volume of TFA to the ubiquitin solution and 40 mM *p*TsOH (final concentration) for 16 h at room temperature. The deprotection reaction was protected from light with end-over-end rotation. Deprotected protein was precipitated with ice-cold ethyl ether followed by a one-time wash of ice-cold ethyl ether. The precipitated protein was refolded using 6 M guanidine hydrochloride and buffer exchanged into a buffer containing 50 mM MES (pH 6.0) and 100 mM NaCl. The deprotected Ub_{1-75}-NCL was then reacted with the cysteine-light (*p*Bpa)PCNA that contains a K164C mutation in a buffer containing 50 mM MES (pH 6.0) and 100 mM NaCl in a molar ratio of 2:1 to generate Ub-(*p*Bpa)PCNA probe. The reaction condition was 4 hours at room temperature protected from light. The protein mixture was directly loaded onto a HiTrap Q anion exchange column (GE Healthcare Life Sciences). The protein was eluted with a 50–1000 mM NaCl gradient in a buffer containing 50 mM Tris-HCl (pH 8.0), 5% glycerol and 1 mM DTT. The peak fractions containing Ub-(*p*Bpa)PCNA were collected and concentrated. (*p*Bpa)^{68}Ub-PCNA probe was generated using (*p*Bpa)$^{68}Ub_{1-75}$ and an untagged cysteine-

light PCNA following a similar procedure as described (58).

Photo-crosslinking of Polη with (*p*Bpa)PCNA or Ub-(*p*Bpa)PCNA and LC-MS/MS analysis

Small-scale photo-crosslinking reaction (10 μl volume) was performed in a crosslinking solution containing 50 mM Tris-HCl (pH 7.5), 10% glycerol and 50 mM NaCl. (*p*Bpa)PCNA or Ub-(*p*Bpa)PCNA probe (trimer) and Polη^{FL} were mixed at a molar concentration ratio of approximately 1:1 and incubated on ice for 30 min. Protein mixture was then photo-crosslinked by UV (365 nm) at 4°C in a 0.75 ml clear microcentrifuge tube (Thermo Fisher Scientific). Samples were then resolved on a 12% SDS-PAGE gel.

For LC-MS/MS analysis of the crosslinked protein bands, an approximately 1:1 molar concentration ratio of (*p*Bpa)PCNA trimer (141 μg) to Polη^{FL} (109 μg), (*p*Bpa)PCNA trimer (154 μg) to Polη^{CC} (96 μg), Ub-(*p*Bpa)PCNA trimer (125 μg) to Polη^{FL} (75 μg) were used for photo-crosslinking reaction. Photo-crosslinking reaction was performed in a buffer containing 50 mM Tris-HCl (pH 7.5), 10% glycerol and 50 mM NaCl. Protein solutions were mixed and incubated in a 0.75 ml clear microcentrifuge tube on ice for 30 min followed by photo-crosslinking with UV at 365 nM for 30 min at 4°C. Samples were then resolved on a 12% SDS-PAGE gel. SDS-PAGE gels were stained and de-stained using the Pierce Silver Stain for Mass Spectrometry kit (Thermo Fisher Scientific) before in-gel digestion. Crosslink bands were excised into small pieces and placed in a 0.75 ml clear microcentrifuge tube. Destaining was performed according to the procedure of the kit. Gel slices were then treated with the addition of 100% acetonitrile with occasional vortex for 5 min followed by removal of the supernatant. The treatment was repeated three times. Gel slices were reduced by a buffer containing 10 mM DTT and 25 mM ammonium bicarbonate at 56°C for 60 min. Alkylation was performed in a buffer containing 55 mM iodoacetamide and 25 mM ammonium bicarbonate at room temperature for 45 min protected from light. Samples were then incubated in a buffer containing 25 mM ammonium bicarbonate with occasional vortex for 10 min. The buffer was then removed and replaced by 100% acetonitrile. The gel slices were then incubated for 10 min with occasional vortex. The ammonium bicarbonate and acetonitrile treatment step was repeated one more time. Acetonitrile was then removed from the tube. Dried gel slices were digested by 4 μg MS grade trypsin (Thermo Fisher Scientific) in a 25 mM ammonium bicarbonate solution at 37°C for 16 h. Tryptic digestion was quenched by the addition of 0.1% formic acid. The supernatant was transferred and kept in a new tube. Extraction of peptides was done by incubating gel slices in 100 μl buffer containing 5% formic acid and 50% acetonitrile for 10 min with occasional vortex followed by another round extraction in 100 μl buffer containing 5% formic acid and 70% acetonitrile for 10 min with occasional vortex. Combined extraction solutions together with kept supernatant were dried by SpeedVac, redissolved in 0.1% formic acid in diH_2O, desalted with Pierce C18 tip (Thermo Fisher Scientific) and SpeedVac dried again before LC-MS/MS analysis. Dried samples were redissolved in 0.1% formic acid in diH_2O. Samples were then analyzed by a nano UHPLC column (15 cm long, 5 μm inner diameter, 3 μm C18 resin) connected to Orbitrap Q-Exactive (Thermo Fisher Scientific) for identification of crosslinked peptides.

Analysis of protein crosslinking sites by MeroX

The Proteome Discoverer 1.4 (Thermo Fisher Scientific) software was used to export mass spectrometry spectra as Mascot generic format (MGF) file. All protein sequences used for the analysis were derived from UniProt (www.uniprot.org). The mass spectrometry spectra were analyzed by MeroX (2.0.1.4) for crosslinked peptides (60–62) in quadratic analysis mode with the following settings: photoactivatable unnatural amino acid *p*Bpa was set as code x in the FASTA file with a composition of $C_{16}H_{13}NO_2$. *p*Bpa was set to be able to crosslink with all twenty amino acids plus methionine sulfoxide and iodoacetamide alkylated cysteine. Trypsin protease was set to cleave C-terminal to lysine or arginine with a maximum of three missed cleavages. Only peptides with a length of 5 to 30 were analyzed. Cysteine alkylation by iodoacetamide was set as a fixed modification. Methionine oxidation was set as a variable modification with a maximum modification number of two. Precision for precursor was set as 4 ppm and precision for fragment ion was set as 6 ppm. The mass range of the peptide was set as 200.0–6000.0 Da. *S*/*N* for the peptide was set as 2. The minimum number of fragments per peptide was set as three. About 1% was used for false discover rate cut-off to filter out low score candidates. Percentage intensity cut off in the prescore setting was set as 30%. The common Repository of Adventitious Proteins (cRAP) database was used to increase the size of the protein sequences to improve the accuracy of the decoy analysis. Decoy database generation was set as shuffling sequences but keeping protease sites for the analysis and decoy database level was set as decoy based on peptide sequence shuffling/reversing for the analysis.

HADDOCK protein–protein docking for generation of the Polη/PCNA model

Protein–protein docking platform HADDOCK2.4 was used for the generation of the Polη catalytic core-PCNA complex model. PCNA structure (PDB: 1PLQ) (27) with a built-in duplex DNA was generated through a superimposition with the PCNA-DNA structure (PDB: 3K4X) (63). This was necessary because the PCNA sequence in the PCNA-DNA structure lacks the C-terminal residues that are important for docking. Apo-Polη^{CC} structure (PDB: 1JIH) (17) or Polη^{CC} structure (PDB: 2R8K) with bound DNA removed (18) were used for docking analysis. Crosslinking residues were used to provide a restraint for the docking. HADDOCK2.4 default settings were used. A 31 base-pair (bp) duplex DNA built using PyMOL was superimposed with the original 10 bp DNA in the PCNA of the docked structure. Final models were generated in PyMOL for illustration. Apo-Polη^{CC} structure (PDB: 1JIH) was used for trapped and carrier conformation while Polη^{CC} structure (PDB: 2R8K) with bound DNA removed was used for active conformation in generating the models. The

yeast Ub-PCNA structure (PDB: 3L10) was superimposed onto the PCNA ring to build in Ub in the trapped and carrier conformation models. In the active conformation model, the structure of human Ub-PCNA (PDB: 3TBL) was used to build in Ub by superimposition of PCNA rings to create the Polη^{CC}-Ub-PCNA model. Human Polη UBZ (PDB: 2I5O) (64) and human Polη PIP (PDB: 2ZVK) (65) were used to model the UBZ and PIP structural components into the Polη^{CC}-Ub-PCNA models.

DNA synthesis by Polη using an abasic site-containing DNA

The DNA synthesis assay was performed using a primer-template DNA substrate containing a 23-mer primer (5′-AG AGG AAG GAG GAG AAG GAG AAG-3′) or a 29-mer primer (5′-AG AGG AAG GAG GAG AAG GAG AAG AAG GAG-3′) annealed to a 100-mer DNA oligo (5′-CGC TTT GCG TAA CTT TTT TTT TTT TTT TTT TTT TCG CGX CTC CTT CTT CTC CTT CTC CTC CTT CCT CTT TTT TTT TTT TTT TTT TTT TTT TTT T-3′) containing an abasic site analog (X), tetrahydrofuran, with biotin on both 5′ and 3′ end of the template DNA (66) at a molar ratio of 1:1. Both DNA primers were labeled with a Cy5 dye at the 5′ end. The annealed primer-template DNA was incubated with a 10-fold molar excess of streptavidin and a 40-fold molar excess of single-stranded DNA-binding protein (SSB, Promega) at room temperature for 30 min. A typical 25 μl assay solution contains 48 nM DNA substrate, 40 nM Polη, 200 nM PCNA, 200 nM RFC, 4 mM ATP (Alfa Aesar) and 400 μM dNTPs (New England Biolabs) in a reaction buffer containing 40 mM Tris-HCl (pH 7.5), 5 mM $MgCl_2$, 150 mM NaCl and 0.1 mg/ml BSA (Thermo Fisher Scientific). A control DNA synthesis assay was done in the same manner but in the absence of PCNA. Components except Polη were mixed on ice and incubated at 37°C for 5 min. Polη was added to initiate the DNA synthesis for 5 min. The reaction was quenched by the addition of 500 mM EDTA and 10% SDS. DNA was extracted by phenol/chloroform extraction and analyzed on a 15% denaturing urea polyacrylamide gel. The gel was imaged using the Cy5 channel of FluorChem Q gel imager (Alpha Innotech).

RESULTS

Photoaffinity crosslinking of (*p*Bpa)PCNA with full-length yeast Polη

In order to probe the interactions of PCNA and Ub-PCNA with Polη, we incorporated a photo-activatable unnatural amino acid *p*Bpa into different positions on the PCNA surface. The photo-activatable crosslinker *p*Bpa was introduced into the PCNA polypeptide by amber codon suppression (Supplementary Figure S1). We successfully expressed and purified ten (*p*Bpa)PCNA species with *p*Bpa introduced at selected positions on PCNA, including 125 and 254 on the front side; 64, 133, 161 and 168 on the rim and 57, 108, 185, 245 on the back side of the PCNA ring (Figure 1B). All (*p*Bpa)PCNA species were expressed in *E. coli* and purified using HisPur cobalt resin followed by HiTrap Q anion-exchange column to a good purity (Supplementary Figure S2A). The identity of these (*p*Bpa)PCNA species was confirmed by ESI-MS (Supplementary Figure S2B–K).

For photo-induced crosslinking, full-length Polη (Polη^{FL}) and (*p*Bpa)PCNA were pre-incubated on ice for 30 min, followed by UV irradiation at 365 nm for 60 min at 4°C. The resulted photo-crosslinking products were resolved on a 12% SDS-PAGE gel and stained with Coomassie blue dye (Supplementary Figure S3). For a comparison, (*p*Bpa)PCNA species alone were also subjected to photo-crosslinking under the same condition (Supplementary Figure S3). For most (*p*Bpa)PCNA species, only minor self-crosslinking was observed except (*p*Bpa)^{185}PCNA for which strong self-crosslinking bands were observed. No self-crosslinking was observed for Polη alone.

To rule out potential non-specific photo-induced crosslinking, BSA was incubated with (*p*Bpa)PCNA species and crosslinked under the same condition and no discernable crosslinking bands between (*p*Bpa)PCNA and BSA were observed for all ten (*p*Bpa)PCNA species tested (Supplementary Figure S4). Furthermore, time-dependent crosslinking was performed for four (*p*Bpa)PCNA species with photo-crosslinker introduced at 64, 125, 245 and 254 position on PCNA (Supplementary Figure S5A). The formation of photo-crosslinking product was found to reach a plateau in approximately 15 min. We also observed increased crosslinking when the concentrations of Polη or PCNA were increased in the crosslinking reactions (Supplementary Figure S5B and S5C).

As shown in Supplementary Figure S3, (*p*Bpa)PCNA/Polη crosslinking bands were observed for *p*Bpa introduced at 64, 108, 125, 161, 168, 245 and 254 position on PCNA when assessed using an SDS-PAGE gel and Coomassie blue staining. For several of the (*p*Bpa)PCNA probes, multiple crosslinking bands were observed, often with one or two dominating crosslinking bands. No discernable crosslinking bands with Polη were observed for *p*Bpa introduced at 57, 133 and 185 position on PCNA. Interestingly, although most *p*Bpa sites on PCNA for which efficient crosslinking was observed are located on the front side (125 and 254) or the rim (64, 161 and 168) of PCNA, two sites (108 and 245) on the back of PCNA ring also afforded efficient crosslinking with Polη. Notably, all sites that did not afford crosslinking, i.e. 57, 133 and 185, are located on the rim (133) or back side (57 and 185) of PCNA. The lack of crosslinking for these sites provides further support for the specific crosslinking between (*p*Bpa)PCNA and Polη.

Identification of Polη crosslinking sites using tandem mass spectrometry

We next used trypsin digestion and mass spectrometry to identify crosslinking sites on Polη^{FL} when incubated with (*p*Bpa)PCNA probes. The crosslinking bands were excised and combined, followed by trypsin digestion and analysis using nano LC-MS/MS to identify potential crosslinking sites. Crosslinked peptides were identified using the software MeroX as described in Materials and Methods section (60–62). We identified multiple crosslinking sites in both the

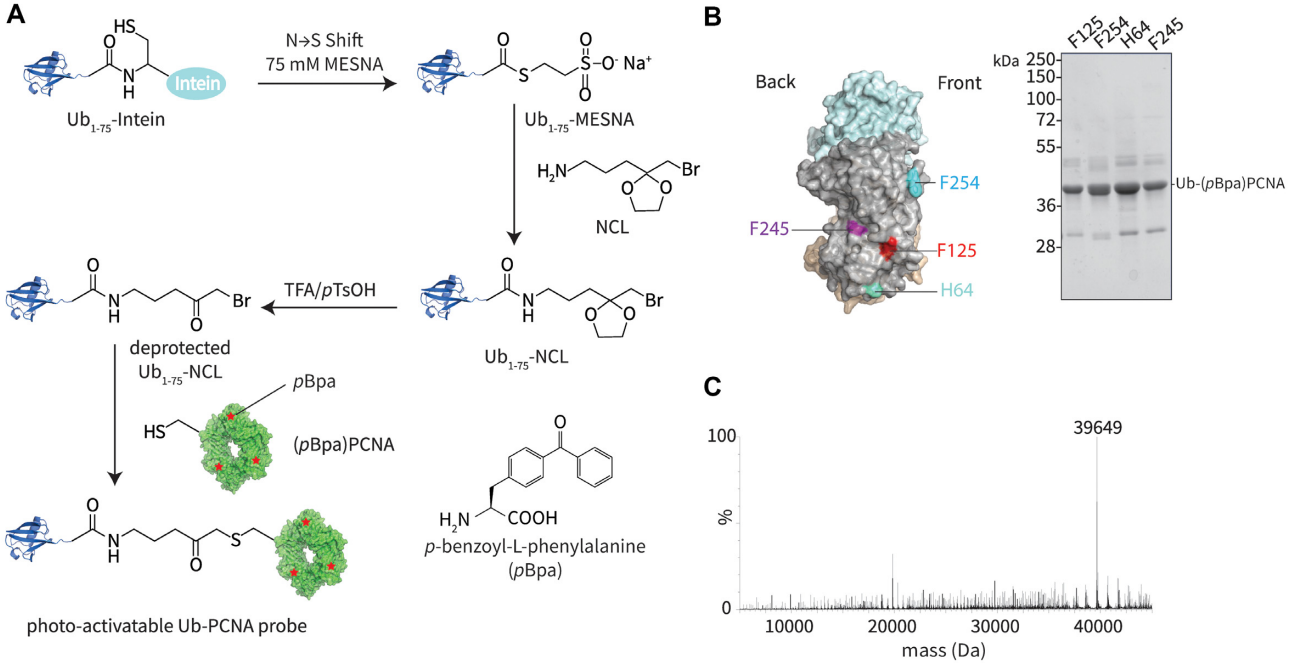

Figure 2. Generation and characterization of photo-activatable Ub-(*p*Bpa)PCNA probes. (**A**) Chemical steps of generating Ub-(*p*Bpa)PCNA probes. The structure of *p*Bpa is illustrated. (**B**) SDS-PAGE gel analysis of the Ub-(*p*Bpa)PCNA probes with *p*Bpa introduced at position 64, 125, 245 and 254. (**C**) ESI-MS characterization of Ub-(*p*Bpa)^{125}PCNA probe. Calculated MW (39,649 Da) of Ub-(*p*Bpa)^{125}PCNA reflects the loss of the N-terminal methionine of PCNA during *Escherichia coli* expression.

Polη catalytic core and the C-terminal region of Polη for several (*p*Bpa)PCNA probes (Supplementary Table S1).

For (*p*Bpa)^{125}PCNA, the peptide 74–82 in the fingers domain of Polη was identified as the highest-ranked peptide by MeroX (Figure 1C). The other top-ranked Polη crosslinked peptides include the Polη PIP motif (a.a. 623–630) (Supplementary Figure S6A) and a Polη peptide (a.a. 597–602) in the disordered region close to the Polη C terminus (Supplementary Figure S6B).

For (*p*Bpa)^{254}PCNA, peptide 451–457 in the LF domain of Polη was found to be crosslinked to (*p*Bpa)^{254}PCNA, with Arg456 being the most likely crosslinking residue (Figure 1D). In addition, peptides in the Polη fingers domain (a.a. 74–82) (Supplementary Figure S6C) and in the Polη disordered region (a.a. 514–527 and 603–615) (Supplementary Figure S6D and S6E) were also found to be crosslinked to *p*Bpa introduced at position 254 on PCNA.

When *p*Bpa was introduced at the back side of PCNA at position 245, a thumb domain peptide (a.a. 352–366) in the Polη catalytic core was identified to be crosslinked to the (*p*Bpa)^{245}PCNA probe (Figure 1E). In addition, a Polη sequence (a.a. 617–622) in a disordered region proceeding the PIP box (a.a. 621–628) was also identified (Supplementary Figure S6F). Notably, a peptide (a.a. 577–589) that partially overlaps with the Polη UBZ domain was found to be crosslinked to (*p*Bpa)^{245}PCNA (Supplementary Figure S6G), suggesting that the only ordered element in the Polη C-terminal region may directly interact with the back side of PCNA. No crosslinking with the Polη UBZ domain was detected when *p*Bpa was introduced to the front side of PCNA (125 or 254). This observation suggests that despite the flexibility of the Polη C-terminal region, its UBZ domain under most circumstances is positioned close to the back side of the PCNA ring. This is in line with the observation that Ub at K164 is positioned toward the back side of the PCNA ring (54).

Generation of Ub-(*p*Bpa)PCNA probes for photo-crosslinking analysis of Polη/Ub-PCNA complex

Photo-activatable Ub-(*p*Bpa)PCNA probes were prepared following a previously reported method (58), except that a K164C (*p*Bpa)PCNA cysteine-light mutant was used (Figure 2A). The chemically ubiquitinated PCNA with a thioether linkage was previously shown to function similarly to the native monoubiquitinated PCNA in stimulating Polη's activity (57). The thioether linkage mimics the isopeptide linkage in the native ubiquitinated PCNA and resists cleavage by reducing agents. By combining chemical protein ubiquitination and photo-activatable unnatural amino acid incorporation, we obtained a set of monoUb-PCNA with *p*Bpa incorporated at selected positions, i.e. 64, 125, 245 and 254, on both sides of the PCNA ring (Figure 2B). All Ub-(*p*Bpa)PCNA probes were purified and characterized by ESI-MS (Figure 2C and Supplementary Figure S7). The strategical positioning of the photo-activatable crosslinker allowed us to systematically interrogate the interaction between Polη and monoubiquitinated PCNA.

Photo-crosslinking of Ub-(*p*Bpa)PCNA with Polη

Ubiquitination of PCNA serves as a signal for recruitment of TLS polymerase Polη to the stalled replicative polymerase holoenzyme complex at the DNA damage site. The

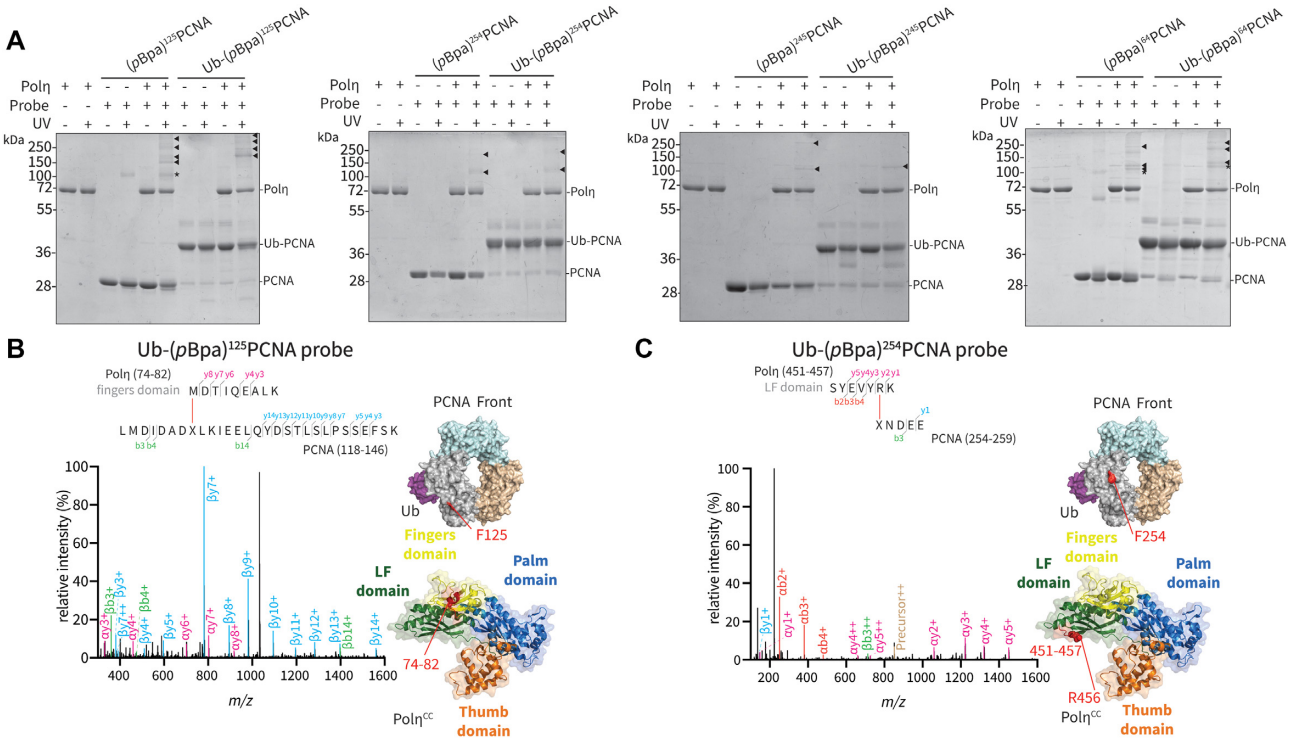

Figure 3. Photo-crosslinking of the full-length Polη with (*p*Bpa)PCNA or Ub-(*p*Bpa)PCNA. (**A**) SDS-PAGE gel showing photo-crosslinking of Polη with (*p*Bpa)PCNA or Ub-(*p*Bpa)PCNA probes with *p*Bpa introduced at 64, 125, 245 or 254 position, respectively. Major crosslinking bands between Polη and (*p*Bpa)PCNA or Ub-(*p*Bpa)PCNA probes are highlighted with a triangle. Probe self-crosslinking bands are indicated with an asterisk. (**B**) A representative MS/MS spectrum of a peptide (a.a. 74–82) in the Polη fingers domain crosslinked to a PCNA peptide containing ^{125}*p*Bpa. X represents *p*Bpa. (**C**) A representative MS/MS spectrum of a peptide (a.a. 451–457) in the Polη LF domain crosslinked to a PCNA peptide containing ^{254}*p*Bpa. X represents *p*Bpa. Yeast Ub-PCNA (PDB: 3L10) and Polη^{CC} (PDB: 2R8K) structures are shown and for clarity only one of the ubiquitins is shown on the homotrimeric Ub-PCNA structure.

interaction between Polη and Ub-PCNA is not fully understood. We selected H64 (rim), F125 (front), F245 (back) and F254 (front) for introducing *p*Bpa into monoubiquitinated PCNA in order to probe the potential interactions between Polη and both sides of Ub-PCNA. All Ub-(*p*Bpa)PCNA probes were tested for photo-crosslinking with BSA control and no significant crosslinking band was observed (Supplementary Figure S8). We compared the crosslinking band pattern of the corresponding (*p*Bpa)PCNA and Ub-(*p*Bpa)PCNA with Polη^{FL} and observed an overall similar labeling pattern with a noticeable upshift of the crosslinking bands (Figure 3A).

We next used trypsin digestion and mass spectrometry to identify the site of crosslinking on Polη when incubated with Ub-(*p*Bpa)PCNA probes (Supplementary Table S1). Interestingly, several Polη residues located in the catalytical core were also found to be crosslinked to Ub-(*p*Bpa)PCNA when *p*Bpa was introduced at position 125 and 254 on PCNA. Particularly, the peptide (a.a. 74–82) in the fingers domain of Polη was found to be crosslinked to Ub-(*p*Bpa)^{125}PCNA (Figure 3B). In addition, peptides in the Polη PIP box (a.a. 623–630) and in the disordered region (a.a. 597–602) were also found to be crosslinked to Ub-(*p*Bpa)^{125}PCNA (Supplementary Figure S9A and S9B). For Ub-(*p*Bpa)^{254}PCNA, Arg456 on the peptide 451–457 in the LF domain of the Polη catalytic core was identified as the major crosslinking site (Figure 3C). Crosslinking sites in the Polη disordered region (a.a. 514–527) and (a.a. 604–615) were also identified (Supplementary Figure S9C and S9D). Overall PCNA monoubiquitination at K164 had a minimal impact on the crosslinking between *p*Bpa introduced at the front side of PCNA and Polη. In comparison, a more profound effect was observed on the crosslinking between *p*Bpa introduced at the back side of PCNA and Polη. Comparing the identified crosslinking sites between Ub-(*p*Bpa)^{245}PCNA and (*p*Bpa)^{245}PCNA, only a sequence near Polη C-terminal PIP box (a.a. 617–622) was found crosslinked to the Ub-(*p*Bpa)^{245}PCNA probe (Supplementary Figure S9E), while the crosslinking sites on the Polη thumb and UBZ domains observed for (*p*Bpa)^{245}PCNA were no longer detected.

We also generated (*p*Bpa)^{68}Ub-PCNA probe, in which *p*Bpa was introduced onto Ub at H68 (Figure 4A). Tandem mass spectrometry analysis of the crosslinking product between (*p*Bpa)^{68}Ub-PCNA and Polη^{FL} identified a peptide in the Polη UBZ domain (a.a. 564–576) as the site of crosslinking with (*p*Bpa)^{68}Ub (Figure 4B). Notably H68 on Ub is juxtaposed to I44 that resides at the center of a hydrophobic patch and was shown to interact with the Polη UBZ domain (67). Our crosslinking result agrees well with the known interaction between Ub and the Polη UBZ domain, which supports the validity of the photo-activatable PCNA or Ub-PCNA probes in mapping their interaction with Polη.

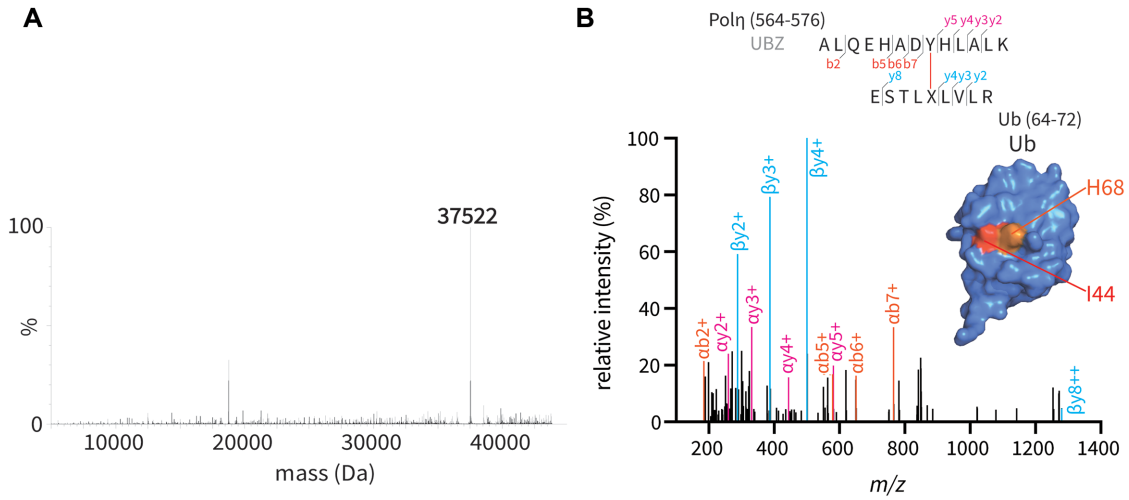

Figure 4. Identified crosslinked peptides between the full-length Polη with (pBpa)^{68}Ub-PCNA probe. (**A**). ESI-MS characterization of (pBpa)^{68}Ub-PCNA probe with incorporated pBpa at position 68 in Ub. The determined MW is in agreement with the calculated MW of 37,522 Da for (pBpa)^{68}Ub-PCNA. (**B**) A representative MS/MS spectrum of a peptide (a.a. 564–576) in the Polη UBZ crosslinked to a Ub-PCNA peptide containing ^{68}pBpa in Ub. X represents pBpa. The position of H68 (orange) and I44 (red) are highlighted in the Ub structure (PDB: 1UBQ).

Characterization of (pBpa)PCNA and Ub-(pBpa)PCNA's interaction with catalytic core of Polη

Photo-crosslinking between the full-length Polη (Polη^{FL}) and (pBpa)PCNA or Ub-(pBpa)PCNA probes revealed a direct interaction between the catalytic core of Polη (Polη^{CC}) with PCNA and Ub-PCNA. Next, we tested crosslinking of Polη^{CC} with (pBpa)PCNA and Ub-(pBpa)PCNA. In (pBpa)^{125}PCNA crosslinking with the Polη^{CC}, we consistently observed a discrete crosslinking band (Figure 5A). Mass spectrometry analysis revealed that the most prominent crosslinking peptide on Polη^{CC} is a.a. 74–82 in the fingers domain of Polη (Figure 5B and Supplementary Table S2), which was also observed in (pBpa)^{125}PCNA crosslinking to the Polη^{FL}. In addition, a Polη peptide located in the palm domain (a.a. 144–163) was identified in Polη^{CC}'s crosslinking to (pBpa)^{125}PCNA.

In addition to (pBpa)^{125}PCNA, crosslinking band with Polη^{CC} was also observed for (pBpa)^{161}PCNA and (pBpa)^{254}PCNA (Supplementary Figure S10), both are located at the front side of the PCNA ring. Among the pBpa sites for which no crosslinking with Polη^{CC} was observed (64, 168 and 245), position 245 is on the back side of PCNA. Thus, the crosslinking between the Polη^{CC} with PCNA is predominantly on its front side. This is in contrast to the Polη^{FL}, for which crosslinking with (pBpa)^{245}PCNA on the back side was observed. This distinction stresses the importance of the C-terminal region of Polη in positioning the Polη^{CC} toward the back side of PCNA.

We also assessed the crosslinking between Polη^{CC} and Ub-(pBpa)PCNA. Among the four Ub-(pBpa)PCNA tested (64, 125, 245 and 254), only Ub-(pBpa)^{125}PCNA was found to crosslink with Polη^{CC} (Supplementary Figure S10). Photo-crosslinking of the Polη^{CC} with (pBpa)PCNA and Ub-(pBpa)PCNA provides further evidence for the direct interaction between Polη^{CC} and the PCNA's front side. The overall weaker crosslinking efficiency observed for Polη^{CC} with (pBpa)PCNA and Ub-(pBpa)PCNA than that of Polη^{FL} agrees with the role of the C-terminal region of Polη^{FL} in tethering Polη^{CC} to the PCNA ring.

Assessing the effect of a potential internal PIP in regulating Polη's activity in TLS

The crosslinking peptide identified by (pBpa)^{254}PCNA or (pBpa)^{254}Ub-PCNA probe revealed a PIP-like sequence ^{512}QKTVVDMF in yeast Polη. To assess the role of the potential internal PIP box in regulating Polη's activity, we generated and purified a truncated Polη$_{1–523}$ that contains the catalytic core and the internal PIP sequence (Supplementary Figure S11A). We also introduced a double mutation, M518A/F519A, into the internal PIP in the full-length Polη sequence. We tested the activity of the Polη species using an abasic site analog, tetrahydrofuran, containing template DNA annealed with a 5′-Cy5 labeled 23-mer or 29-mer DNA primer (Supplementary Figure S11B) in the presence of PCNA and RFC. We found that for the truncated Polη$_{1–523}$ harboring the potential internal PIP, little nucleotide incorporation opposite the abasic site was observed, similar to the Polη^{CC} (Supplementary Figure S11C). This represents a drastic decrease compared to the full-length Polη (Supplementary Figure S11C). Notably when Polη^{FL} with mutations (M518A/F519A) introduced into the internal PIP sequence was tested in the DNA synthesis assay, a clear decrease in nucleotide incorporation opposite the abasic site was observed when compared to the WT Polη^{FL} (Supplementary Figure S11C). Nonetheless, the observed incorporation activity was appreciably higher than that of the Polη^{CC} and Polη$_{1–523}$. When PCNA was left out of the DNA synthesis assay, little nucleotide incorporation opposite the abasic site was observed for all four Polη constructs despite comparable nucleotide incorporation up to the lesion site (Supplementary Figure S11D), suggesting that the difference observed in Supplementary Figure S11C

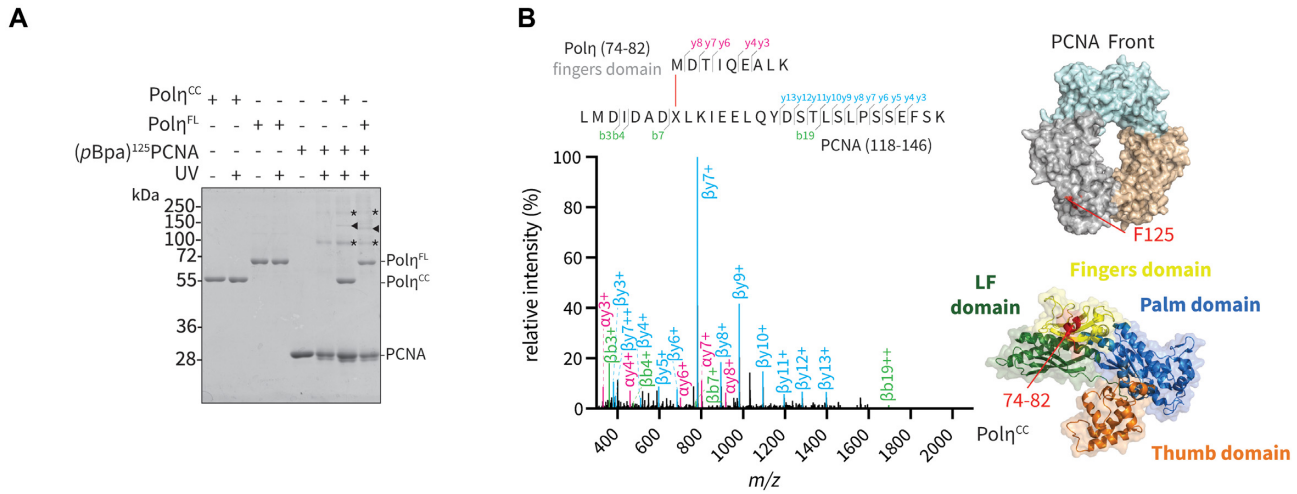

Figure 5. Photo-crosslinking of the Polη catalytic core (Polη^{CC}) with (*p*Bpa)^{125}PCNA or Ub-(*p*Bpa)^{125}PCNA. (**A**) Photo-crosslinking of Polη^{CC} with (*p*Bpa)^{125}PCNA in comparison to the full-length Polη (Polη^{FL}). Major crosslinking bands between Polη with the (*p*Bpa)PCNA probe are highlighted with a triangle. Probe self-crosslinking bands are indicated with an asterisk. (**B**) A representative MS/MS spectrum of a peptide (a.a. 74–82) in the Polη fingers domain crosslinked to a PCNA peptide containing ^{125}*p*Bpa. X represents *p*Bpa. Surface-rendered structures of PCNA (PDB: 1PLQ) and Polη^{CC} (PDB: 2R8K) showing the site of *p*Bpa incorporation (F125) on the front side of PCNA ring and the identified peptide a.a. 74–82 in the fingers domain, respectively.

is PCNA dependent. These observations support the importance of the internal PIP in stimulating Polη^{FL}'s activity in the presence of PCNA.

Probing the Polη-interaction sites on PCNA in stimulating Polη's activity

We next introduced mutations to the Polη interaction sites on PCNA that were revealed by our crosslinking study. Three PCNA mutants with mutation on the PCNA back side (F245A), IDCL (L126A/I128A), C-terminal region (P252A/K253A) were purified and assessed using the same Polη DNA synthesis assay using the abasic site-containing DNA. The PCNA IDCL (L126A/I128A) and C-terminal (P252A/K253A) mutations were selected because of their closeness to the identified crosslinking sites (125 and 254), respectively. Furthermore, these PCNA mutants were previously characterized and found to retain normal interaction with RFC (68). ESI-MS and SDS-PAGE were used to verify the mutant PCNAs (Supplementary Figures S12A–D and S13A). Interestingly, while no effect was observed for the back side mutant PCNA (F245A) on Polη's activity of nucleotide incorporation opposite the abasic site, the IDCL mutant PCNA (L126A/I128A) or C-terminal region mutant PCNA (P252A/K253A) showed drastically reduced ability in stimulating Polη's activity (Supplementary Figure S13B), suggesting the importance of the identified interactions at PCNA's IDCL or C-terminal region in modulating Polη's activity in TLS.

DISCUSSION

Structural details of the Ub-PCNA/Polη complex have remained scarce. By combining the chemical ubiquitination method and unnatural amino acid approach, we generated a set of (*p*Bpa)PCNA and Ub-(*p*Bpa)PCNA probes that enabled a detailed mapping of the interaction sites between yeast Polη and PCNA (Supplementary Figure S14). It has been established that Polη binds PCNA through its C-terminal PIP peptide at a surface cleft close to the IDCL on PCNA. In agreement with this notion, (*p*Bpa)^{125}PCNA in which *p*Bpa is located on the IDCL afforded strong crosslinking with the full-length Polη. Notably, we also captured crosslinking between the Polη catalytic core and (*p*Bpa)PCNA. Depending on the position of *p*Bpa introduced on PCNA, the fingers domain, thumb domain and LF domain were found to directly interact with PCNA. Furthermore, our finding provides a direct evidence that Polη interacts with the back sides of the PCNA ring when *p*Bpa was introduced at position 245 and 108 on the back of PCNA.

Previous structural studies of both archaeal and bacterial TLS polymerases interacting with their processivity factors have led to a model in which the TLS polymerase may be held in a 'carrier' conformation by interacting with PCNA (or β clamp) until a major conformation change to bring the polymerase catalytic core close to the bound DNA for synthesis. In *E. coli*, the LF domain of the Y-family polymerase Pol IV binds to the opposite edges of the β clamp dimer in an orientation that would place Pol IV in an unproductive conformation (69). In archaea, the co-crystal structure of *Saccharolobus solfataricus* Y-family polymerase Dpo4 with its heterotrimeric PCNA showed that the full-length Dpo4 adopts an extended, inactive carrier conformation (70). In addition to the interaction between the Dpo4 PIP peptide and the PCNA1 subunit, supplementary binding sites mainly located on the rim of PCNA were also identified between PCNA and the Dpo4 thumb, fingers and palm domains. The last 11 residues of Dpo4 in the LF domain (a.a. 240–352) that contain the PIP box become ordered when bound to PCNA1. The contacts between Dpo4 with PCNA1 are primarily between positively

charged residues located close to the DNA-binding cleft of Dpo4 and negatively charged residues of PCNA1. Interestingly, three major contacts that we found between the catalytic core of Polη with PCNA are also close to the DNA binding site in Polη (Supplementary Figure S15). Notably, the full-length Dpo4 was found to adopt very different conformations in the DNA-bound (71) and the Dpo4-PCNA1 complexes, largely due to a flexible hinge region between the Dpo4 LF domain and its PIP box sequence.

Compared to Dpo4, yeast Polη harbors a much longer C-terminal disordered region (a.a. 509–632) with an embedded UBZ domain (a.a. 549–582) and a C-terminal PIP box sequence (a.a. 621–628). Thus, in Polη, a flexible conformation of the catalytic core relative to the interacting PCNA is likely due to a longer disordered C-terminal region in the full-length Polη. Indeed, we found interaction sites near the Polη PIP box (a.a. 617–622) and in the UBZ domain (a.a. 577–589) with the back side of PCNA, as well as two sites (a.a. 514–527 and 616–630) in the Polη disordered region interacting with the front side of PCNA. These findings suggest that the interaction between the C-terminal region of Polη and PCNA is more extensive than that was previously thought, not just through the PIP box and the PCNA front surface. We envision that these interactions are likely to be transient in nature. In fact, transient interactions are found to often involve disordered regions in proteins across the whole proteome (72,73). It is believed that the linear motifs (LM) (sometimes more than one) in the disordered region may contribute to the interaction of the disordered peptide with well-folded protein partners. The extensive disordered region in Polη and the multiple interactions detected with PCNA in this study provides an example of transient interactions involving disordered regions in the DNA replication system.

We performed a multiple sequence alignment of *Saccharomyces cerevisiae* Polη (POLH_YEAST) with *Drosophila melanogaster* Polη (POLH_DROME), *Homo sapiens* Polη (POLH_HUMAN), *Arabidopsis thaliana* Polη (POLH_ARATH), *S. solfataricus* Dpo4 (DPO4_SACS2) and *E. coli* Pol IV (DPO4_ECOLI) (Supplementary Figure S16). Overall, the polymerase catalytic core containing fingers, palm, thumb and LF domains is well conserved among these polymerases except several sequence insertions observed in the yeast Polη sequence. We mapped the Polη peptides crosslinked to PCNA to the aligned sequence, including a.a. 74–82 in fingers domain, a.a. 352–366 in thumb domain, a.a. 451–457 in LF domain and a.a. 514–527 that follows the LF domain (Supplementary Figure S16). The crosslinked peptide (a.a. 74–82) in the yeast Polη is conserved among the four aligned Polη sequences from *H. sapiens*, *Drosophila*, *S. cerevisiae* and *Arabidopsis*. In comparison, the a.a. 352–366 and a.a. 451–457 regions are diverged, in line with the largely loop structure observed for these two regions in the yeast Polη catalytical core. Although the sequences following the LF domain of the polymerases highly diverge, we noted that a.a. 514–527 (crosslinked predominantly to ^{254}pBpa on PCNA) right after the LF domain contains a major part of a PIP-like sequence ^{512}QKTVVDMF. This sequence (a.a. 512–519) aligns well with the known *H. sapiens* Polη PIP1 sequence and *S. solfataricus* Dpo4 C-terminal PIP box. Thus, yeast Polη likely harbors an internal PIP-like sequence (^{512}QKTVVDMF) juxtaposed to the LF domain (a.a. 393–508). The well-established PIP box at the C-terminus of *S. cerevisiae* Polη (a.a. 621–628) was found to be crosslinked to *p*Bpa introduced at position 125 on PCNA, which is located on the IDCL right next to the PCNA pocket known to bind the hydrophobic plug donated by the PIP box. Our crosslinking result from (*p*Bpa)^{125}PCNA is in good agreement with the known binding mode of the Polη C-terminal PIP box to the well-defined pocket on PCNA surface. Importantly, (*p*Bpa)^{254}PCNA crosslinking with full-length yeast Polη revealed a previously unknown interaction between a putative yeast Polη internal PIP box with the PCNA surface surrounding Phe254. Recently, a second PIP (^{593}FGEKRLLF) in yeast Polη was reported, suggesting a complex mechanism that the Polη PIP boxes may play different roles during TLS (74). Notably, we identified a Polη ^{597}RLLFSR peptide being crosslinked with (*p*Bpa)^{125}PCNA or Ub-(*p*Bpa)^{125}PCNA.

To assess the functional importance of the potential internal PIP-like sequence in yeast Polη (^{512}QKTVVDMF), we introduced a double mutation (M518A/F519A) to Polη^{FL} and observed a significant decrease in Polη^{FL}'s activity in incorporating nucleotide opposite an abasic site in the template DNA. This observation agrees with a previous report of a high UV sensitivity observed for yeast strains harboring Polη mutant with consecutive a.a. 513–522 or a.a. 518–527 mutated to alanine or glycine (48). Interestingly, a truncated Polη$_{1–523}$ that harbors the internal PIP in addition to the catalytic core lost activity in inserting nucleotide opposite the abasic site in the presence of PCNA. These observations suggest that the internal PIP alone is not sufficient in orienting Polη's catalytic core for productive TLS synthesis and the Polη C-terminal region is indispensable. Disruption in the Polη internal PIP and its interaction with PCNA likely destabilizes the productive conformation of Polη in the complex and led to suboptimal TLS synthesis.

Given that the Polη internal PIP sequence likely binds next to F254 on PCNA based on our crosslinking results, we introduced mutations (P252A/K253A) into the PCNA sequence right before F254. We found that the DNA synthesis activity of Polη^{FL} opposite the abasic site was drastically reduced in the presence of mutant PCNA P252A/K253A compared to PCNA with an intact C-terminal sequence. Interestingly, the same PCNA C-terminal region was reported to interact with the yeast DNA ligase Cdc9 (68). Our result supports a direct interaction between the C-terminal region of PCNA and its binding partners through a PIP or PIP-like sequence. In fact a previous co-crystal structure of a human Polη PIP-containing peptide bound to human PCNA showed that the Polη peptide lies close to the PCNA C-terminal peptide region (65).

Our crosslinking results revealing the interactions of the Polη catalytic core with different sites on PCNA suggest that Polη may adopt different conformations in the complex with PCNA or Ub-PCNA. Given that a high-resolution crystal structure of Polη catalytic core is available, we carried out a protein–protein docking analysis between PCNA trimer and the Polη catalytic core guided by the identified photo-crosslinking sites between PCNA and Polη using HADDOCK (75). A top docking model generated us-

ing PCNA (Phe245) and Polη (Arg357) crosslinking as a restraint placed Polη in a trapped conformation with the polymerase active site distant from the built-in double-stranded DNA threaded through the cavity of the PCNA ring (Figure 6A). Separately, a docking model of Polη and PCNA using Polη Met74's interaction with PCNA Phe125 as a restraint revealed a binding mode that likely represents a carrier conformation without significant clash with the built-in DNA (Figure 6A). This model also avoids a potential clash between Polη and Ub on the back side of PCNA (*vide infra*). This model somewhat resembles that of the Pol IV LF binding to the *E. coli* β clamp in which the LF and likely the body of the Pol IV protrude away from the edge of the clamp.

Notably, when we docked the Polη catalytic core with PCNA using the Arg456 (Polη LF domain) and Phe254 (front of PCNA) crosslinking as a restraint, in addition to a number of the models showing that the Polη catalytic core is edged away from the DNA threading through the PCNA central cavity, one model showed a potential active conformation considering the positioning of bound DNA relative to the Polη active site (Figure 6A). By building in a B-form duplex DNA using PyMOL with superimposition of the modeled DNA onto the duplex DNA found in the PCNA/DNA cocrystal structure (63), the Polη active site accommodates the end of the duplex DNA well while allowing the threading of the DNA duplex region through the central cavity of PCNA. Thus, this model likely represents a productive conformation of the PCNA/Polη complex on the DNA substrate. The fact that we observed multiple conformations of the catalytic core of Polη relative to the PCNA ring while maintaining the interaction between PCNA Phe254 and Polη Arg456 suggests that the Polη–PCNA interaction is fluid and only when Polη engages the DNA it is locked down to an active conformation for DNA synthesis. Notably, when we introduced the *S. cerevisiae* Polδ structure (PDB: 7KC0) into the trapped or carrier Polη-PCNA conformation by superimposing the recently reported *S. cerevisiae* Polδ-PCNA complex (76) with the modeled Polη-PCNA structure using the common PCNA structure, we observed no steric clash between Polη and Polδ (Supplementary Figure S17A and S17B). In comparison, we cannot introduce the Polδ structure into the modeled Polη-PCNA structure in the active conformation without a clash between the two polymerases. This suggests that Polη may bind to PCNA in a trapped or carrier conformation simultaneously with Polδ on PCNA and a polymerase exchange is needed to replace Polδ by Polη for productive TLS.

When comparing the crosslinking of FL Polη with Ub-(*p*Bpa)PCNA versus (*p*Bpa)PCNA using SDS-PAGE gel analysis of the crosslinked bands, we observed largely comparable crosslinking band pattern except for some upshift of the bands. Our mass spectrometry analysis is in line with this observation with similar crosslinking peptides identified on Polη when *p*Bpa was introduced at position 125 and 254 on the front side of PCNA. Thus, no steric clash between Polη and Ub on the back side of PCNA is expected in the carrier and active conformations, as reflected in the respective models (Figure 6A and B). One notable difference was observed for *p*Bpa introduced at position 245 on the back side of PCNA. For (*p*Bpa)^{245}PCNA, three Polη peptides were identified, including ^{352}QSDYDRSTSNIDPLK in the thumb domain, ^{617}QVTSSK in the disordered C-terminal region and ^{577}LSEGLNGAEESSK in the UBZ domain. When Ub-(*p*Bpa)^{245}PCNA was used in crosslinking with Polη^{FL}, we were only able to detect the Polη C-terminal peptide ^{617}QVTSSK. One possible interpretation of the observed difference is that the presence of Ub located at the back side of PCNA may destabilize the Polη thumb domain from binding to the back of the PCNA ring, likely due to a steric effect. In addition, the interaction between Ub and the Polη UBZ domain may also seclude UBZ from direct interaction with the back side of PCNA at position 245. Agreeing with this notion, when we superimposed the split Ub-PCNA crystal structure (54) with the Polη/PCNA docking models, a steric clash between the thumb domain in the catalytic core of Polη with Ub was observed in the trapped conformation, but not in the carrier and active conformations (Figure 6B).

As PCNA serves as a central platform of DNA replication, lesion bypass and DNA damage repair, the (*p*Bpa)PCNA or Ub-(*p*Bpa)PCNA probes described in this study may be used to understand the dynamic, multicomponent protein complexes important for these DNA transactions. In addition to Polη, the interaction between PCNA and other TLS polymerases (Polζ, κ and ι) and the replicative DNA polymerases (Polδ and Polε) can also be readily interrogated with this set of (*p*Bpa)PCNA or Ub-(*p*Bpa)PCNA probes. In addition to monoubiquitin modification, other types of PCNA modification such as SUMOylation and polyubiquitination can also be incorporated into the probes to investigate the role of these types of modifications in regulating PCNA's interactions with the respective partner proteins. In addition, these (*p*Bpa)PCNA or Ub-(*p*Bpa)PCNA probes can be used to identify new PCNA binding proteins from more complex systems such as cell lysates through photo-crosslinking and pulldown. One advantage of the photoaffinity-capturing is that transient protein interactions evading conventional affinity-based pulldown are more readily captured through covalent bonding. Together with the proteomics approaches (60–62,77,78), the identification of interacting proteins and possibly site(s) of interaction between PCNA and its binding partners in a complex cell lysate system becomes feasible. Lastly, the (*p*Bpa)PCNA or Ub-(*p*Bpa)PCNA probes may also be used to form stable protein complexes with binding partners to enable high-resolution X-ray crystallography and cryo-EM studies to afford full details of the PCNA-containing protein complexes.

DATA AVAILABILITY

Existing protein sequences are from UniProt (www.uniprot.org). Protein crystal structures are from PDB (www.rcsb.org). Protein–protein docking tool HADDOCK2.4 is available for use with registration (haddock.science.uu.nl). Protein–protein crosslink analysis tool MeroX is a software for Windows operating system (www.stavrox.com). Mass spectrometry data and protein structure models have been deposited into the DYRAD database (doi.org/10.5061/dryad.nk98sf7s3).

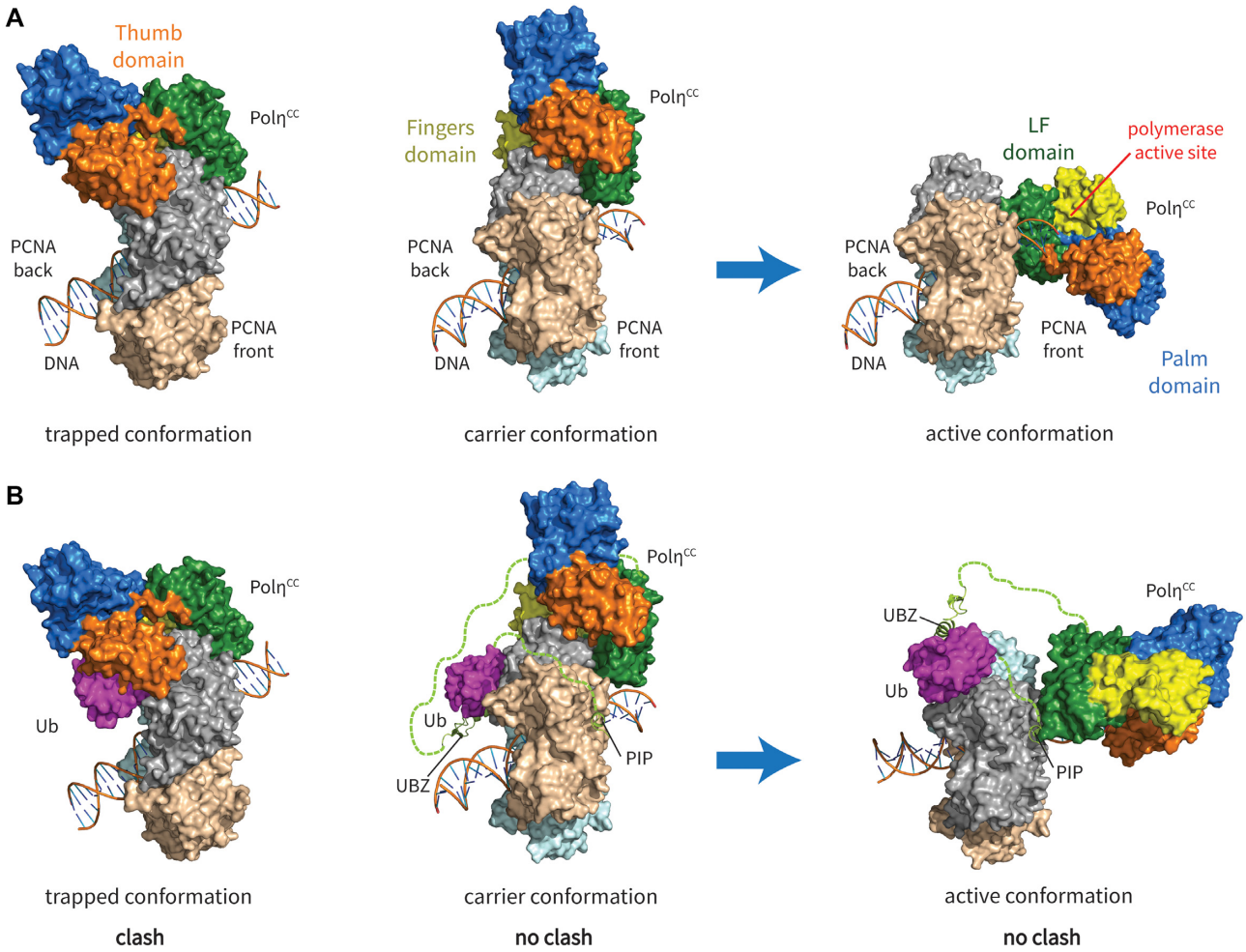

Figure 6. Model of the *S. cerevisiae* Polη/PCNA or Polη/Ub-PCNA complex in different conformations. (**A**) Model of the Polη thumb domain interacting with the back side of PCNA reflecting a trapped conformation (left), interaction of fingers domain of Polη with the rim of PCNA reflecting a carrier conformation (middle) and Polη LF domain interacting with the front side of PCNA in an active conformation (right). These models were generated using the residue-specific crosslinking information as a restraint (see 'Materials and Methods' and 'Results' section). The structure of yeast PCNA (PDB: 1PLQ) and the Polη catalytic core (PDB: 1JIH for the trapped or carrier conformation and 2R8K for the active conformation) were used for HADDOCK modeling and PyMOL illustration. (**B**) Model of the Polη/Ub-PCNA in the trapped (left), carrier (middle) and active (right) conformation. The structure of yeast Ub-PCNA (PDB: 3L10) was used to build in Ub on the docked PCNA for trapped or carrier conformation and the structure of human Ub-PCNA (PDB: 3TBL) was used to build in Ub on the docked PCNA for active conformation in the PyMOL illustration. Steric clash between Polη and Ub was only observed in the trapped conformation. Polη PIP (PDB: 2ZVK), UBZ (PDB: 2I5O) and C-terminal disordered region (dashed line) are used to illustrate the possible position of the structural elements in the models.

SUPPLEMENTARY DATA

Supplementary Data are available at NAR Online.

ACKNOWLEDGEMENTS

We thank PapaNii Asare-Okai in the Mass Spectrometry Facility at University of Delaware for his help in the mass spectrometry analysis. pEVOL-pBpF plasmid was a gift from Peter Schultz (Addgene plasmid # 31190). We also thank Sandra Körner for the help with plasmid construction and Weijun Gui for providing valuable suggestions.

FUNDING

National Institutes of Health (NIH) [R01 GM129468 to Z.Z.]; National Institute of General Medical Sciences [P30 GM110758, P20 GM104316]. Funding for open access charge: NIH [GM129468].
Conflict of interest statement. None declared.

REFERENCES

1. Ohmori,H., Friedberg,E.C., Fuchs,R.P., Goodman,M.F., Hanaoka,F., Hinkle,D., Kunkel,T.A., Lawrence,C.W., Livneh,Z., Nohmi,T. *et al.* (2001) The Y-family of DNA polymerases. *Mol. Cell*, **8**, 7–8.
2. Goodman,M.F. (2002) Error-prone repair DNA polymerases in prokaryotes and eukaryotes. *Annu. Rev. Biochem.*, **71**, 17–50.
3. Prakash,S., Johnson,R.E. and Prakash,L. (2005) Eukaryotic translesion synthesis DNA polymerases: specificity of structure and function. *Annu. Rev. Biochem.*, **74**, 317–353.
4. Waters,L.S., Minesinger,B.K., Wiltrout,M.E., D'Souza,S., Woodruff,R.V. and Walker,G.C. (2009) Eukaryotic translesion polymerases and their roles and regulation in DNA damage tolerance. *Microbiol. Mol. Biol. Rev.*, **73**, 134–154.

5. Sale,J.E., Lehmann,A.R. and Woodgate,R. (2012) Y-family DNA polymerases and their role in tolerance of cellular DNA damage. *Nat. Rev. Mol. Cell Biol.*, **13**, 141–152.
6. Yang,W. (2014) An overview of Y-Family DNA polymerases and a case study of human DNA polymerase η. *Biochemistry*, **53**, 2793–2803.
7. Masutani,C., Kusumoto,R., Yamada,A., Dohmae,N., Yokoi,M., Yuasa,M., Araki,M., Iwai,S., Takio,K. and Hanaoka,F. (1999) The XPV (xeroderma pigmentosum variant) gene encodes human DNA polymerase eta. *Nature*, **399**, 700–704.
8. Johnson,R.E., Kondratick,C.M., Prakash,S. and Prakash,L. (1999) hRAD30 mutations in the variant form of xeroderma pigmentosum. *Science*, **285**, 263–265.
9. Hoege,C., Pfander,B., Moldovan,G.L., Pyrowolakis,G. and Jentsch,S. (2002) RAD6-dependent DNA repair is linked to modification of PCNA by ubiquitin and SUMO. *Nature*, **419**, 135–141.
10. Stelter,P. and Ulrich,H.D. (2003) Control of spontaneous and damage-induced mutagenesis by SUMO and ubiquitin conjugation. *Nature*, **425**, 188–191.
11. Bienko,M., Green,C.M., Crosetto,N., Rudolf,F., Zapart,G., Coull,B., Kannouche,P., Wider,G., Peter,M., Lehmann,A.R. *et al.* (2005) Ubiquitin-binding domains in Y-family polymerases regulate translesion synthesis. *Science*, **310**, 1821–1824.
12. Johnson,R.E., Prakash,S. and Prakash,L. (1999) Efficient bypass of a thymine-thymine dimer by yeast DNA polymerase, Poleta. *Science*, **283**, 1001–1004.
13. Haracska,L., Yu,S.L., Johnson,R.E., Prakash,L. and Prakash,S. (2000) Efficient and accurate replication in the presence of 7,8-dihydro-8-oxoguanine by DNA polymerase eta. *Nat. Genet.*, **25**, 458–461.
14. Ling,H., Boudsocq,F., Plosky,B.S., Woodgate,R. and Yang,W. (2003) Replication of a cis-syn thymine dimer at atomic resolution. *Nature*, **424**, 1083–1087.
15. Carlson,K.D. and Washington,M.T. (2005) Mechanism of efficient and accurate nucleotide incorporation opposite 7,8-dihydro-8-oxoguanine by Saccharomyces cerevisiae DNA polymerase eta. *Mol. Cell. Biol.*, **25**, 2169–2176.
16. McCulloch,S.D., Kokoska,R.J., Garg,P., Burgers,P.M. and Kunkel,T.A. (2009) The efficiency and fidelity of 8-oxo-guanine bypass by DNA polymerases delta and eta. *Nucleic Acids Res.*, **37**, 2830–2840.
17. Trincao,J., Johnson,R.E., Escalante,C.R., Prakash,S., Prakash,L. and Aggarwal,A.K. (2001) Structure of the catalytic core of S. cerevisiae DNA polymerase eta: implications for translesion DNA synthesis. *Mol. Cell*, **8**, 417–426.
18. Alt,A., Lammens,K., Chiocchini,C., Lammens,A., Pieck,J.C., Kuch,D., Hopfner,K.P. and Carell,T. (2007) Bypass of DNA lesions generated during anticancer treatment with cisplatin by DNA polymerase eta. *Science*, **318**, 967–970.
19. Biertümpfel,C., Zhao,Y., Kondo,Y., Ramón-Maiques,S., Gregory,M., Lee,J.Y., Masutani,C., Lehmann,A.R., Hanaoka,F. and Yang,W. (2010) Structure and mechanism of human DNA polymerase eta. *Nature*, **465**, 1044–1048.
20. Silverstein,T.D., Johnson,R.E., Jain,R., Prakash,L., Prakash,S. and Aggarwal,A.K. (2010) Structural basis for the suppression of skin cancers by DNA polymerase eta. *Nature*, **465**, 1039–1043.
21. Ummat,A., Rechkoblit,O., Jain,R., Roy Choudhury,J., Johnson,R.E., Silverstein,T.D., Buku,A., Lone,S., Prakash,L., Prakash,S. *et al.* (2012) Structural basis for cisplatin DNA damage tolerance by human polymerase η during cancer chemotherapy. *Nat. Struct. Mol. Biol.*, **19**, 628–632.
22. Nakamura,T., Zhao,Y., Yamagata,Y., Hua,Y.J. and Yang,W. (2012) Watching DNA polymerase η make a phosphodiester bond. *Nature*, **487**, 196–201.
23. Patra,A., Banerjee,S., Johnson Salyard,T.L., Malik,C.K., Christov,P.P., Rizzo,C.J., Stone,M.P. and Egli,M. (2015) Structural Basis for Error-Free Bypass of the 5-N-Methylformamidopyrimidine-dG Lesion by Human DNA Polymerase η and Sulfolobus solfataricus P2 Polymerase IV. *J. Am. Chem. Soc.*, **137**, 7011–7014.
24. Patra,A., Zhang,Q., Lei,L., Su,Y., Egli,M. and Guengerich,F.P. (2015) Structural and kinetic analysis of nucleoside triphosphate incorporation opposite an abasic site by human translesion DNA polymerase η. *J. Biol. Chem.*, **290**, 8028–8038.
25. Lau,W.C., Li,Y., Zhang,Q. and Huen,M.S. (2015) Molecular architecture of the Ub-PCNA/Pol η complex bound to DNA. *Sci. Rep.*, **5**, 15759.
26. Moldovan,G.L., Pfander,B. and Jentsch,S. (2007) PCNA, the maestro of the replication fork. *Cell*, **129**, 665–679.
27. Krishna,T.S., Kong,X.P., Gary,S., Burgers,P.M. and Kuriyan,J. (1994) Crystal structure of the eukaryotic DNA polymerase processivity factor PCNA. *Cell*, **79**, 1233–1243.
28. Jónsson,Z.O., Hindges,R. and Hübscher,U. (1998) Regulation of DNA replication and repair proteins through interaction with the front side of proliferating cell nuclear antigen. *EMBO J.*, **17**, 2412–2425.
29. Mailand,N., Gibbs-Seymour,I. and Bekker-Jensen,S. (2013) Regulation of PCNA-protein interactions for genome stability. *Nat. Rev. Mol. Cell Biol.*, **14**, 269–282.
30. Choe,K.N. and Moldovan,G.L. (2017) Forging ahead through darkness: PCNA, still the principal conductor at the replication fork. *Mol. Cell*, **65**, 380–392.
31. Freudenthal,B.D., Ramaswamy,S., Hingorani,M.M. and Washington,M.T. (2008) Structure of a mutant form of proliferating cell nuclear antigen that blocks translesion DNA synthesis. *Biochemistry*, **47**, 13354–13361.
32. Dieckman,L.M. and Washington,M.T. (2013) PCNA trimer instability inhibits translesion synthesis by DNA polymerase η and by DNA polymerase δ. *DNA Repair (Amst.)*, **12**, 367–376.
33. Kondratick,C.M., Boehm,E.M., Dieckman,L.M., Powers,K.T., Sanchez,J.C., Mueting,S.R. and Washington,M.T. (2016) Identification of new mutations at the PCNA subunit interface that block translesion synthesis. *PLoS One*, **11**, e0157023.
34. Hershko,A. and Ciechanover,A. (1998) The ubiquitin system. *Annu. Rev. Biochem.*, **67**, 425–479.
35. Scheffner,M., Nuber,U. and Huibregtse,J.M. (1995) Protein ubiquitination involving an E1-E2-E3 enzyme ubiquitin thioester cascade. *Nature*, **373**, 81–83.
36. Chen,Z.J. and Sun,L.J. (2009) Nonproteolytic functions of ubiquitin in cell signaling. *Mol. Cell*, **33**, 275–286.
37. Komander,D. and Rape,M. (2012) The ubiquitin code. *Annu. Rev. Biochem.*, **81**, 203–229.
38. Hu,H. and Sun,S.C. (2016) Ubiquitin signaling in immune responses. *Cell Res.*, **26**, 457–483.
39. Yang,K., Weinacht,C.P. and Zhuang,Z. (2013) Regulatory role of ubiquitin in eukaryotic DNA translesion synthesis. *Biochemistry*, **52**, 3217–3228.
40. Kannouche,P.L., Wing,J. and Lehmann,A.R. (2004) Interaction of human DNA polymerase eta with monoubiquitinated PCNA: a possible mechanism for the polymerase switch in response to DNA damage. *Mol. Cell*, **14**, 491–500.
41. Plosky,B.S., Vidal,A.E., Fernandez de Henestrosa,A.R., McLenigan,M.P., McDonald,J.P., Mead,S. and Woodgate,R. (2006) Controlling the subcellular localization of DNA polymerases iota and eta via interactions with ubiquitin. *EMBO J.*, **25**, 2847–2855.
42. Zhuang,Z., Johnson,R.E., Haracska,L., Prakash,L., Prakash,S. and Benkovic,S.J. (2008) Regulation of polymerase exchange between Poleta and Poldelta by monoubiquitination of PCNA and the movement of DNA polymerase holoenzyme. *PNAS*, **105**, 5361–5366.
43. Masuda,Y., Piao,J. and Kamiya,K. (2010) DNA replication-coupled PCNA mono-ubiquitination and polymerase switching in a human in vitro system. *J. Mol. Biol.*, **396**, 487–500.
44. Chang,D.J. and Cimprich,K.A. (2009) DNA damage tolerance: when it's OK to make mistakes. *Nat. Chem. Biol.*, **5**, 82–90.
45. Andersen,P.L., Xu,F. and Xiao,W. (2008) Eukaryotic DNA damage tolerance and translesion synthesis through covalent modifications of PCNA. *Cell Res.*, **18**, 162–173.
46. Parker,J.L. and Ulrich,H.D. (2009) Mechanistic analysis of PCNA poly-ubiquitylation by the ubiquitin protein ligases Rad18 and Rad5. *EMBO J.*, **28**, 3657–3666.
47. Ulrich,H.D. and Jentsch,S. (2000) Two RING finger proteins mediate cooperation between ubiquitin-conjugating enzymes in DNA repair. *EMBO J.*, **19**, 3388–3397.
48. Powers,K.T., Elcock,A.H. and Washington,M.T. (2018) The C-terminal region of translesion synthesis DNA polymerase η is partially unstructured and has high conformational flexibility. *Nucleic Acids Res.*, **46**, 2107–2120.

49. Haracska,L., Kondratick,C.M., Unk,I., Prakash,S. and Prakash,L. (2001) Interaction with PCNA is essential for yeast DNA polymerase eta function. *Mol. Cell*, **8**, 407–415.
50. Duong,P.T.M., Bui,A.T.N., Kim,S.O., Park,H.S., Seo,Y.S. and Choi,B.S. (2020) The interaction between ubiquitin and yeast polymerase η C terminus does not require the UBZ domain. *FEBS Lett.*, **594**, 1726–1737.
51. Indiani,C., McInerney,P., Georgescu,R., Goodman,M.F. and O'Donnell,M. (2005) A sliding-clamp toolbelt binds high- and low-fidelity DNA polymerases simultaneously. *Mol. Cell*, **19**, 805–815.
52. Kath,J.E., Jergic,S., Heltzel,J.M., Jacob,D.T., Dixon,N.E., Sutton,M.D., Walker,G.C. and Loparo,J.J. (2014) Polymerase exchange on single DNA molecules reveals processivity clamp control of translesion synthesis. *Proc. Natl. Acad. Sci. U. S. A.*, **111**, 7647–7652.
53. Boehm,E.M., Spies,M. and Washington,M.T. (2016) PCNA tool belts and polymerase bridges form during translesion synthesis. *Nucleic Acids Res.*, **44**, 8250–8260.
54. Freudenthal,B.D., Gakhar,L., Ramaswamy,S. and Washington,M.T. (2010) Structure of monoubiquitinated PCNA and implications for translesion synthesis and DNA polymerase exchange. *Nat. Struct. Mol. Biol.*, **17**, 479–484.
55. Zhang,Z., Zhang,S., Lin,S.H., Wang,X., Wu,L., Lee,E.Y. and Lee,M.Y. (2012) Structure of monoubiquitinated PCNA: implications for DNA polymerase switching and Okazaki fragment maturation. *Cell Cycle*, **11**, 2128–2136.
56. Chin,J.W., Martin,A.B., King,D.S., Wang,L. and Schultz,P.G. (2002) Addition of a photocrosslinking amino acid to the genetic code of Escherichiacoli. *Proc. Natl. Acad. Sci. U.S.A.*, **99**, 11020–11024.
57. Yang,K., Li,G., Gong,P., Gui,W., Yuan,L. and Zhuang,Z. (2016) Chemical protein ubiquitylation with preservation of the native cysteine residues. *ChemBioChem*, **17**, 995–998.
58. Gong,P., Davidson,G.A., Gui,W., Yang,K., Bozza,W.P. and Zhuang,Z. (2018) Activity-based ubiquitin-protein probes reveal target protein specificity of deubiquitinating enzymes. *Chem. Sci.*, **9**, 7859–7865.
59. Chen,J., Ai,Y., Wang,J., Haracska,L. and Zhuang,Z. (2010) Chemically ubiquitylated PCNA as a probe for eukaryotic translesion DNA synthesis. *Nat. Chem. Biol.*, **6**, 270–272.
60. Götze,M., Pettelkau,J., Schaks,S., Bosse,K., Ihling,C.H., Krauth,F., Fritzsche,R., Kühn,U. and Sinz,A. (2012) StavroX–a software for analyzing crosslinked products in protein interaction studies. *J. Am. Soc. Mass Spectrom.*, **23**, 76–87.
61. Iacobucci,C., Götze,M., Ihling,C.H., Piotrowski,C., Arlt,C., Schäfer,M., Hage,C., Schmidt,R. and Sinz,A. (2018) A cross-linking/mass spectrometry workflow based on MS-cleavable cross-linkers and the MeroX software for studying protein structures and protein-protein interactions. *Nat. Protoc.*, **13**, 2864–2889.
62. Götze,M., Iacobucci,C., Ihling,C.H. and Sinz,A. (2019) A simple cross-linking/mass spectrometry workflow for studying system-wide protein interactions. *Anal. Chem.*, **91**, 10236–10244.
63. McNally,R., Bowman,G.D., Goedken,E.R., O'Donnell,M. and Kuriyan,J. (2010) Analysis of the role of PCNA-DNA contacts during clamp loading. *BMC Struct. Biol.*, **10**, 3.
64. Bomar,M.G., Pai,M.T., Tzeng,S.R., Li,S.S. and Zhou,P. (2007) Structure of the ubiquitin-binding zinc finger domain of human DNA Y-polymerase eta. *EMBO Rep.*, **8**, 247–251.
65. Hishiki,A., Hashimoto,H., Hanafusa,T., Kamei,K., Ohashi,E., Shimizu,T., Ohmori,H. and Sato,M. (2009) Structural basis for novel interactions between human translesion synthesis polymerases and proliferating cell nuclear antigen. *J. Biol. Chem.*, **284**, 10552–10560.
66. Yang,K., Gong,P., Gokhale,P. and Zhuang,Z. (2014) Chemical protein polyubiquitination reveals the role of a noncanonical polyubiquitin chain in DNA damage tolerance. *ACS Chem. Biol.*, **9**, 1685–1691.
67. Woodruff,R.V., Bomar,M.G., D'Souza,S., Zhou,P. and Walker,G.C. (2010) The unusual UBZ domain of Saccharomyces cerevisiae polymerase η. *DNA Repair (Amst.)*, **9**, 1130–1141.
68. Vijayakumar,S., Chapados,B.R., Schmidt,K.H., Kolodner,R.D., Tainer,J.A. and Tomkinson,A.E. (2007) The C-terminal domain of yeast PCNA is required for physical and functional interactions with Cdc9 DNA ligase. *Nucleic Acids Res.*, **35**, 1624–1637.
69. Bunting,K.A., Roe,S.M. and Pearl,L.H. (2003) Structural basis for recruitment of translesion DNA polymerase Pol IV/DinB to the beta-clamp. *EMBO J.*, **22**, 5883–5892.
70. Xing,G., Kirouac,K., Shin,Y.J., Bell,S.D. and Ling,H. (2009) Structural insight into recruitment of translesion DNA polymerase Dpo4 to sliding clamp PCNA. *Mol. Microbiol.*, **71**, 678–691.
71. Chu,X., Liu,F., Maxwell,B.A., Wang,Y., Suo,Z., Wang,H., Han,W. and Wang,J. (2014) Dynamic conformational change regulates the protein-DNA recognition: an investigation on binding of a Y-family polymerase to its target DNA. *PLoS Comput. Biol.*, **10**, e1003804.
72. Kim,P.M., Sboner,A., Xia,Y. and Gerstein,M. (2008) The role of disorder in interaction networks: a structural analysis. *Mol. Syst. Biol.*, **4**, 179.
73. Perkins,J.R., Diboun,I., Dessailly,B.H., Lees,J.G. and Orengo,C. (2010) Transient protein-protein interactions: structural, functional, and network properties. *Structure*, **18**, 1233–1243.
74. Ripley,B.M., Reusch,D.T. and Washington,M.T. (2020) Yeast DNA polymerase η possesses two PIP-like motifs that bind PCNA and Rad6-Rad18 with different specificities. *DNA Repair (Amst.)*, **95**, 102968.
75. van Zundert,G.C.P., Rodrigues,J.P.G.L., Trellet,M., Schmitz,C., Kastritis,P.L., Karaca,E., Melquiond,A.S.J., van Dijk,M., de Vries,S.J. and Bonvin,A.M.J.J. (2016) The HADDOCK2.2 Web Server: user-friendly integrative modeling of biomolecular complexes. *J. Mol. Biol.*, **428**, 720–725.
76. Zheng,F., Georgescu,R.E., Li,H. and O'Donnell,M.E. (2020) Structure of eukaryotic DNA polymerase δ bound to the PCNA clamp while encircling DNA. *Proc. Natl. Acad. Sci. U.S.A.*, **117**, 30344–30353.
77. Yang,B., Wu,Y.J., Zhu,M., Fan,S.B., Lin,J., Zhang,K., Li,S., Chi,H., Li,Y.X., Chen,H.F. *et al.* (2012) Identification of cross-linked peptides from complex samples. *Nat. Methods*, **9**, 904–906.
78. Chen,Z.L., Meng,J.M., Cao,Y., Yin,J.L., Fang,R.Q., Fan,S.B., Liu,C., Zeng,W.F., Ding,Y.H., Tan,D. *et al.* (2019) A high-speed search engine pLink 2 with systematic evaluation for proteome-scale identification of cross-linked peptides. *Nat. Commun.*, **10**, 3404.